Engineering Journal issn: 0125-8281

Article

Comparison of Different Synthesis Schemes for Production of Sodium Methoxide from Methanol and Sodium Hydroxide

Natthiyar Aeamsuksai[1,a], Thirawat Mueansichai[2,b,*], Pongtorn Charoensuppanimit[3,4,c], Pattaraporn Kim-Lohsoontorn[1,4,d], Farid Aiouache[5,e], and Suttichai Assabumrungrat[1,4,f]

1 Center of Excellence in Catalysis and Catalytic Reaction Engineering, Department of Chemical Engineering, Faculty of Engineering, Chulalongkorn University, Bangkok 10330, Thailand
2 Department of Chemical and Materials Engineering, Faculty of Engineering, Rajamangala University of Technology Thanyaburi, Pathumtani 12110, Thailand
3 Control and Systems Engineering Research Laboratory, Department of Chemical Engineering, Faculty of Engineering, Chulalongkorn University, Bangkok 10330, Thailand
4 Bio-Circular-Green-economy Technology & Engineering Center, BCGeTEC, Department of Chemical Engineering, Faculty of Engineering, Chulalongkorn University, Bangkok 10330, Thailand
5 Department of Engineering, Lancaster University, Lancaster LA1 4YW, United Kingdom
E-mail: [a]siriporn1083@gmail.com, [b]thirawat.m@en.rmutt.ac.th (Corresponding author), [c]Pongtorn.Ch@chula.ac.th, [d]Pattaraporn.K@chula.ac.th, [e]f.aiouache@lancaster.ac.uk, [f]Suttichai.A@chula.ac.th

Abstract. This research investigates the process simulation of sodium methoxide ($NaOCH_3$) synthesis from methanol (CH_3OH) and sodium hydroxide (NaOH) under three synthesis schemes: schemes A, B, and C. Scheme A consisted of one equilibrium reactor and two distillation columns, scheme B one reactive distillation column and one distillation column, and scheme C one reactive distillation column and pervaporation membrane. The simulation parameters included CH_3OH/NaOH feed flow ratio (1.2-1.6), number of stages (5-30), bottom flow rate (1400-1600 kg/h), and feed stage location (5, 10, 15, 20, 21, 22, 23, and 24). The simulation parameters were varied to determine the optimal $NaOCH_3$ synthetic conditions under different schemes with 0.01 wt% water content, maximum 45 wt% $NaOCH_3$, and the lowest total energy consumption. The results showed that scheme C had the lowest total energy consumption (34.25 GJ/h) under the optimal synthetic condition of 1.4 for CH_3OH/NaOH feed flow ratio, 25 for the number of stages, 1550 kg/h for the bottom flow rate, and the 24th feed stage location, with the $NaOCH_3$ flow rate of 675 kg/h. Scheme C thus holds promising potential as an energy-efficient alternative for synthesis of $NaOCH_3$. The novelty of this research lies in the use of pervaporation membrane in place of distillation column to separate CH_3OH from water and to lower energy consumption and capital cost.

Keywords: Sodium methoxide, methanol, sodium hydroxide, reactive distillation, pervaporation, process simulation.

ENGINEERING JOURNAL Volume 24 Issue 6
Received 20 July 2020
Accepted 7 November 2020
Published 30 November 2020
Online at https://engj.org/
DOI:10.4186/ej.2020.24.6.63

DOI:10.4186/ej.2020.24.6.63

1. Introduction

Sodium methoxide ($NaOCH_3$) is a high-performance alkoxide catalyst that is primarily used in the biodiesel production from waste cooking oil [1], waste chicken fat [2], palm oil [3], canola oil [4], as an intermediary in 1G-biodiesel [5], and enzymatic saccharification enhancer [6].

In biodiesel production, 25-30 wt% $NaOCH_3$ in methanol (CH_3OH) is used as homogeneous catalyst for transesterification reaction [7]. $NaOCH_3$ is a more effective alternative to alkaline metal hydroxides to improve the yield and purity of biodiesel [1]. Existing $NaOCH_3$ synthesis technologies include the reactor-distillation-distillation system [8, 9] and reactive distillation-distillation scheme [10-12]. Sodium hydroxide (NaOH) is commonly used as the precursor for industrial-scale production of $NaOCH_3$ due to low cost and low toxicity.

In [13], reactive distillation was used to enhance dimethyl carbonate synthesis. The reactive distillation was also used to convert vegetable oil into biodiesel [14, 15]. In [7], different $NaOCH_3$ synthetic strategies, including reactive distillation, were investigated and results compared [7].

The final stage of $NaOCH_3$ synthesis involves separating CH_3OH from water. The distillation technology is commonly utilized to separate between water and the raw material (CH_3OH) which is recycled to the synthetic system. The construction of a distillation column requires substantial financial investments. As a result, pervaporation technology was proposed to separate the material from water [16-20].

In [16], pervaporation was used to esterify organic acids and improve the conversion of the reactants. In [17], the reactive distillation augmented with pervaporation was used to synthesize ethyl tert-butyl ether (ETBE) from ethanol and tert-butyl alcohol. The pervaporation efficiently removed water from the bottom product, enhancing the fraction of ETBE in the top product. In [18], the reactive distillation integrated with zeolite NaA membrane-based pervaporation was utilized to etherify tert-amyl alcohol into tert-amyl ethyl ether. The integrated scheme increased the tert-amyl ethyl ether yield by 10 %. The pervaporation was also used to separate bioethanol [19] and biodiesel-CH_3OH mixture [20].

The reactor-distillation-distillation and reactive distillation-distillation technologies are commonly used in biodiesel production. However, the reactor-distillation-distillation technology suffers from limited equilibrium conversion which results in low single-pass conversion and high energy consumption (i.e., operating cost) due to high amounts of unreacted raw material (CH_3OH), requiring multiple recycles. Meanwhile, the reactive distillation-distillation scheme predominantly suffers from high energy consumption due to high amounts of unreacted CH_3OH.

As a result, this research proposes a novel reactive distillation-pervaporation technology which requires neither additional reactor nor second distillation column, resulting in lower capital cost. The proposed distillation-pervaporation technology also reduces the amounts of unreacted CH_3OH and multiple recycling, thereby lowering energy consumption.

Specifically, this research investigates the process simulation of $NaOCH_3$ synthesis from CH_3OH and NaOH under three synthesis schemes: schemes A, B, and C. Scheme A consisted of one equilibrium reactor and two distillation columns, scheme B one reactive distillation column and one distillation column, and scheme C one reactive distillation column and pervaporation membrane. The simulation parameters included CH_3OH/NaOH feed flow ratio (1.2, 1.3, 1.4, 1.5, 1.6), number of stages (5, 10, 15, 20, 25, 30), bottom flow rate (1400, 1450, 1500, 1550, 1600 kg/h), and feed stage location (5, 10, 15, 20, 21, 22, 23, and 24). The simulation parameters were varied to determine the optimal $NaOCH_3$ synthetic conditions under schemes A, B, and C, with 0.01 wt% water content, maximum 45 wt% $NaOCH_3$, and lowest total energy consumption.

2. Modeling and Simulation

Simulations were carried out by using ASPEN Plus to determine the optimal $NaOCH_3$ synthetic conditions that minimize the energy consumption of schemes A, B, and C, given 0.01 wt% water content and maximum 45 wt% $NaOCH_3$.

2.1. Reaction Model

$NaOCH_3$ is synthesized by reversible exothermic reaction which is expressed in Eq. (1).

$$CH_3OH + NaOH \leftrightarrow NaOCH_3 + H_2O \quad (1)$$

It is assumed that a hydroxide-methoxide ionic equilibrium (Eq. (2)) is achieved once CH_3OH and NaOH species are mixed [19].

$$CH_3OH + OH^- \leftrightarrow CH_3O^- + H_2O \quad (2)$$

In terms of ion activities (a), the equilibrium constant of the hydroxide-methoxide ionic equilibrium (K) is expressed in Eq. (3).

$$K = \frac{a(x)_{OCH_3^-}\, a(x)_{H_2O}}{a(x)_{CH_3OH}\, a(x)_{OH^-}} \quad (3)$$

The temperature-dependent equilibrium constant (K) is expressed in Eq. (4). Equation (4) was derived from the linear regression of the experimental data in [7, 21].

$$\ln K = -4.374 + 1751/T \quad (4)$$

where K is the chemical equilibrium constant and T is the system temperature in Kelvin. In Eq. (4), the equilibrium constant (K) decreases with increase in the

system temperature due to the exothermicity of the reaction.

2.2. Process Modeling

The vapor-liquid equilibrium calculations under schemes A, B, and C were performed using the electrolyte non-random two-liquid with Redlich-Kwong equation of state (eNRTL-RK) model. The eNRTL-RK model is ideal for an electrolyte system for ionic species in asymmetric reference state [7, 22]. The eNRTL model can describe the interaction between electrolyte molecules in liquid phase, and the RK model is used to characterize the non-ideal behavior of vaporized molecules in gas phase. The interactions between water and CH_3OH; and between water and $NaOCH_3$ were from the ASPEN Plus database, while the interaction between $NaOCH_3$ and CH_3OH was from [7].

The MESH (material balance, vapor-liquid equilibrium equations, mole fraction summations, and heat balance) model was used to characterize the reactive distillation-pervaporation process (scheme C). In scheme C, the pervaporation unit was used to separate CH_3OH from water using nonporous membrane and CH_3OH was recycled into the system.

Table 1 tabulates the simulated $NaOCH_3$ synthesis schemes: schemes A, B, and C. Under schemes A, B, and C, the total pressure of the ordinary (RadFrac) and reactive distillation columns (RadFrac) was 1 atm, and the NaOH concentration in the NaOH feed stream was 50 wt% in aqueous solution with a flow rate of 999.5 kg/h. Given the assumptions, the $NaOCH_3$ flow rate was 675 kg/h (or 5.4 kt/y). The demand for the catalyst $NaOCH_3$ of a large-scale biodiesel production plant in Europe was 300 kt/y, suggesting the huge market potential for $NaOCH_3$ [23].

Under scheme C, the pervaporation membrane was of hydrophilic type. The membrane performance was determined by the permeate flux, separation factor, and pervaporation separation index. The membrane performance was affected by the membrane polymer arrangement, membrane porosity, interaction between permeate molecules and the membrane, and diffusion of the components [28]. Existing studies on pervaporation utilized the pervaporation technology in dehydration of organic mixture, azeotropic separation, and flavor recovery [24-27]. The permeate flux is defined by Eqs. (5) and (6) [24].

$$J = J_i / \omega_{iP} \quad (5)$$

$$J_i = Q_i \Delta p_i \quad (6)$$

where J is total permeate flux, J_i is the partial flux of component i, ω_{iP} is the mass fraction in the permeate (kg/kg), Q_i is the permeance or pressure normalized flux [29], and Δp_i is the driving force expressed by partial pressure.

The separation factor (α) of the membrane is calculated by Eq. (7), where y and x are permeate and feed composition [24].

$$\alpha_{ab} = \frac{y_a / y_b}{x_a / x_b} \quad (7)$$

Table 1. Simulated $NaOCH_3$ synthesis schemes.

	Scheme A	Scheme B	Scheme C
Prediction models	ENRTL-RK	ENRTL-RK	ENRTL-RK + MESH
Number of operating units	3 units	2 units	2 units
Reaction reactor	REQUIL	RadFrac[b]	RadFrac[b]
$NaOCH_3$ separator	RadFrac[a]	RadFrac[b]	RadFrac[b]
CH_3OH separator	RadFrac[a]	RadFrac[a]	Pervaporation membrane

Note: [a] denotes the ordinary distillation column, and [b] denotes the reactive distillation column.

Scheme A consisted of an equilibrium reactor and two distillation columns for separation of $NaOCH_3$ and CH_3OH.

Scheme B consisted of one reactive distillation column and one ordinary distillation column.

Scheme C consisted of one reactive distillation column and one pervaporation.

The pervaporation separation index (PSI) is expressed by Eq. (8) [24].

$$PSI = J \cdot \alpha \quad (8)$$

The permeate flux, separation factor and PSI of scheme C were based on [24], and the results were validated by ASPEN Plus prior to use.

3. Results and Discussion

3.1. Simulation Results under Scheme A

Figure 1 illustrates the schematic of scheme A, and Table 2 tabulates the initial operating condition of feed and distillation column (DIST-2) of scheme A. The optimal CH_3OH/NaOH feed flow ratio in S-505 that maximized the $NaOCH_3$ yield was determined by varying the feed flow ratio between 1, 1.5, 2, 2.5, 3, 3.5, and 4, given the DIST-1 reflux ratio of 0.001 [7].

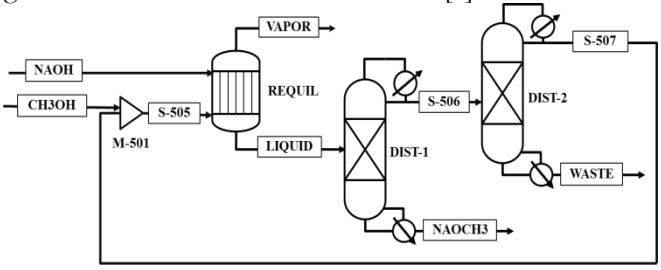

Fig. 1. The schematic of $NaOCH_3$ synthesis under scheme A.

Table 2. Initial operating condition of feed and distillation column (DIST-2) of $NaOCH_3$ synthesis under scheme A.

Parameters	Values
Pressure (atm)	1
Temperature of reactor (˚C)	55
NaOH solution feed rate (kg/h)	999.5
NaOH solution feed temperature (˚C)	30
CH_3OH make-up feed temperature (˚C)	30
DIST-2	
Pressure (atm)	1
Theoretical number of stages	34
Condenser	Partial-vapor
Distillate to feed ratio	0.7841
Reflux ratio	0.8495
Feed stage location	24

Figure 2 shows the effect of CH_3OH/NaOH feed flow ratio on the composition of product (water, CH_3OH, and $NaOCH_3$) and the reboiler duty of scheme A, given the reflux ratio of 0.001. The results revealed that increased CH_3OH/NaOH feed flow ratio had no effect on the $NaOCH_3$ yield but improved the purity of $NaOCH_3$ as the water content decreased. The reboiler duty was positively correlated with the CH_3OH/NaOH feed flow ratio.

Figure 3 (a) illustrates the effect of CH_3OH/NaOH feed flow ratio on the water content under variable reflux ratios (R) of the first distillation column (DIST-1) of scheme A (R = 0.001, 0.1 0.4, and 0.8). The higher the reflux ratio, the higher the water content in the product. The finding was attributable to the non-vaporization of $NaOCH_3$ salt, unlike water and CH_3OH. The lowest water content in the product was achieved under CH_3OH/NaOH feed flow ratio of 4 (Fig. 3 (a)). Figure 3 (b) shows the effect of reflux ratio on water content, given the CH_3OH/NaOH feed flow ratio of 4. The lowest water content was realized under the reflux ratio of 0.001, given the CH_3OH/NaOH feed flow ratio of 4.

Given the reflux ratio (R) of 0.001, DIST-1 of scheme A was operated without condenser to minimize water contamination in $NaOCH_3$. The water content in $NaOCH_3$ should not exceed 0.1 wt% to avoid reversible reaction [10]. The water content was below 0.1 wt% at the CH_3OH/NaOH feed flow ratio of 4 and reflux ratio of 0.001 (Figs. 3 (a)-(b)), with the energy consumption of 2229.37 GJ/h (Fig. 2). Table 3 presents the optimal feed condition of $NaOCH_3$ synthesis under scheme A.

3.2. Simulation Results under Scheme B

The feed and product conditions of the reactive distillation column (D-501) and distillation column (D-502) under scheme B were based on [10]. The values were validated by ASPEN Plus and results tabulated Table 4.

Figure 4 illustrates the schematic of $NaOCH_3$ synthesis under scheme B. Under scheme B, 27 g/h of 50 wt% NaOH in aqueous solution (stream 504) was fed at 1 atm and 75 ˚C into the upper section of the reactive distillation column (D-501). Meanwhile, 54 g/h of CH_3OH at 1 atm and 30 ˚C mixed with recycled CH_3OH (478 g/h; stream 507) was fed at 1 atm and 61 ˚C (stream 505) into the lower section of D-501.

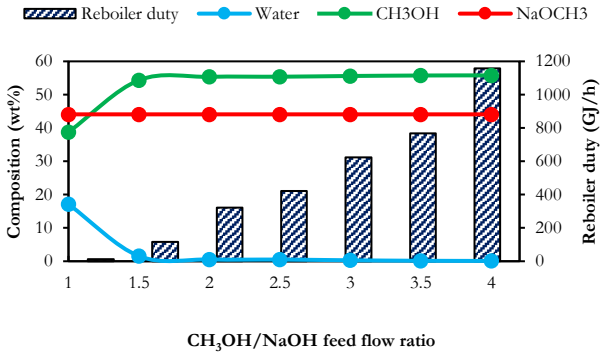

Fig. 2. Effect of CH_3OH/NaOH feed flow ratio on the composition of product and reboiler duty of scheme A, given the reflux ratio of 0.001.

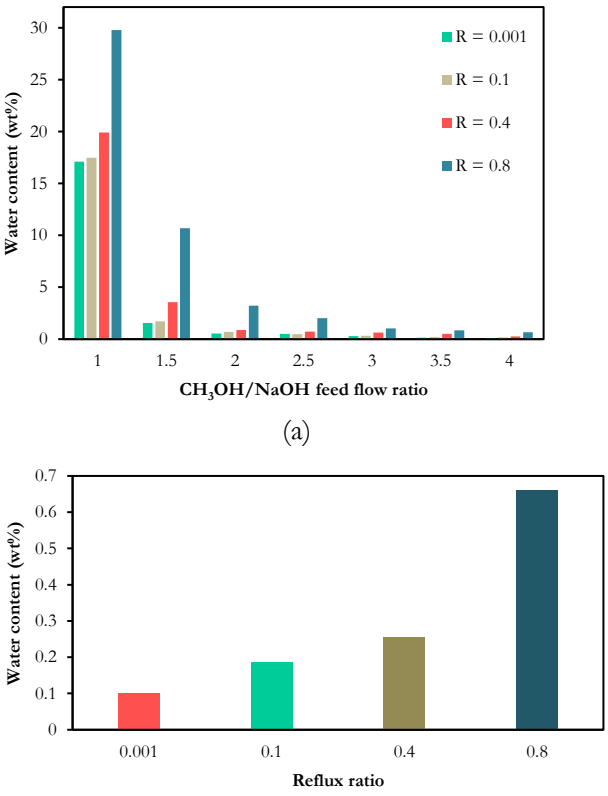

Fig. 3. Water content in the product under scheme A: a) effect of CH_3OH/NaOH feed flow ratio given variable reflux ratios (R), b) effect of reflux ratio given the CH_3OH/NaOH feed flow ratio of 4.

Table 3. The optimal feed condition of $NaOCH_3$ synthesis under scheme A.

Parameters	Values
NaOH solution feed rate (kg/h)	999.5
CH_3OH make-up feed rate (kg/h)	4,000
$NaOCH_3$ flow rate (kg/h)	675 (43.55 wt%)
DIST-1	
Pressure (atm)	1
Theoretical number of stages	15
Condenser	Partial-vapor
Reflux ratio	0.001
Bottom flow rate (kg/h)	1,550
Feed stage location	14
Energy consumption (GJ/h)	2,229.37

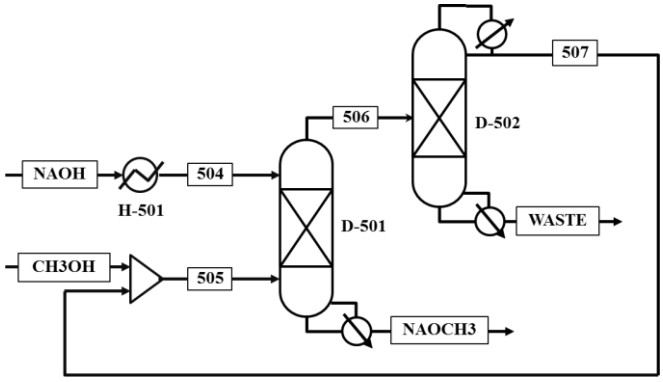

Fig. 4 The schematic of $NaOCH_3$ synthesis under scheme B.

D-501 was operated at 1 atm without condenser to minimize water contamination. The distillate from D-501 (top product) was fed into the ordinary distillation column (D-502) via stream 506 to separate CH_3OH from water. The separated CH_3OH (top product of D-502) was recycled via stream 507 [10]. The bottom product of D-501 was $NaOCH_3$.

The simulated reflux ratio, total number of stages, and feed stage location of D-502 were 1.3, 29, and 25th stage, respectively, given 1 atm pressure. As a result, the simulated total number of stages of D-501 was 20, consistent with [10].

Table 4 tabulates the simulated feed and product conditions of D-501 and D-502 under scheme B. The simulation results were consistent with [10], with discrepancies between the water content in the distillate of D-502 (30 ppm for [10] and 4.1 ppm for the simulation) and the CH_3OH content in the bottom product of D-502 (1 for [10] and 0.2 wt% for the simulation). The water content was below the 0.1 wt% threshold, indicating no reversible reaction.

Under scheme B, the simulation parameters were varied to determine the optimal $NaOCH_3$ synthetic condition with 0.01 wt% water content, maximum 45 wt% $NaOCH_3$, and lowest energy consumption. The simulation parameters were CH_3OH/NaOH feed flow ratio, number of stages, bottom flow rate, and feed stage location. The CH_3OH/NaOH feed flow ratio was varied between 1.2, 1.3, 1.4, 1.5, and 1.6; the number of stages between 5, 10, 15, 20, 25, and 30; the bottom flow rate between 1400, 1450, 1500, 1550, and 1650 kg/h; the feed stage location between 5, 10, 15, 20, 21, 22, 23, and 24. Table 5 tabulates the initial operating condition of feed and distillation column (D-502) under scheme B. Under this scheme (Fig. 4), the CH_3OH feed flow rate (stream 505) was varied, given the NaOH feed flow rate (50 wt% aqueous solution) of 999.5 kg/h (stream 504). The operating condition of D-502, given 1 atm pressure, was of 0.6456 for the reflux ratio, 0.8471 for the distillate-to-mass feed ratio, 30 for the total number of stages, and 20th stage for the feed location, NaOH solution feed temperature of 75 ˚C, and CH_3OH make-up feed temperature of 30 ˚C.

Figures 5 (a)-(f) illustrate the effect of number of stages (5-30) and bottom flow rate (1400-1600 kg/h) of D-501 of scheme B on the concentrations of $NaOCH_3$ and water, given the CH_3OH/NaOH feed flow ratio of 1.2 – 1.6. In Fig. 5 (a), the number of stages and the CH_3OH/NaOH feed flow ratio (1.2 – 1.6) had no effect on the yield of $NaOCH_3$. However, the bottom flow rate was inversely correlated with the $NaOCH_3$ concentration. To maintain $NaOCH_3$ in liquid phase, the maximum concentration of $NaOCH_3$ in the product was 45 wt% [8]. In Fig. 5(a), the maximum $NaOCH_3$ concentration was reached under the bottom flow rate of 1550 kg/h.

Figures 5 (b)-(f) show the effect of number of stages (5-30) and bottom flow rate (1400-1600 kg/h) of D-501 of scheme B on the water content, given the CH_3OH/NaOH feed flow ratios of 1.2, 1.3, 1.4, 1.5, and 1.6. Overall, the water content increased with increase in the bottom flow rate. In addition, the water content in NaOCH3 should be lower than 0.1 wt% to minimize the reversible reaction [9].

In Figs. 5 (b)-(c), the water content exceeded 0.1 wt%, rendering the CH_3OH/NaOH feed flow ratios of 1.2 and 1.3 non-ideal. In Figs. 5 (d)-(f), the water content was below 0.1 wt%, given the CH_3OH/NaOH feed flow ratios of 1.4, 1.5, and 1.6 and the bottom flow rates between 1500-1600 kg/h. In this research, the CH_3OH/NaOH feed flow ratio of 1.4 was adopted for scheme B due to the least CH_3OH required.

Figures 6 (a)-(e) show the effect of number of stages (5-30) and bottom flow rate (1400-1600 kg/h) on total energy consumption of scheme B, given the CH_3OH/NaOH feed flow ratios of 1.2, 1.3, 1.4, 1.5, and 1.6. The energy consumption of D-501 (solid bar) and D-502 (shaded bar) decreased as the bottom flow rate increased.

Under scheme B, given the desirable end-product with 0.01 wt% water content and maximum 45 wt% $NaOCH_3$, the lowest total energy consumption of 35.13 GJ/h was achieved under the bottom flow rate of 1550 kg/h, CH_3OH/NaOH feed flow ratio of 1.4, and the number of stages of 25 for D-501 and D-502.

In Fig. 7, given the bottom flow rate of 1550 kg/h, CH_3OH/NaOH feed flow ratio of 1.4, and the number of stages of 25 for D-501, the 24th feed stage location

DOI:10.4186/ej.2020.24.6.63

exhibited the water content less than 0.1 wt%. Table 6 summarizes the optimal feed and product conditions of $NaOCH_3$ synthesis under scheme B.

Table 4. The simulated feed and product conditions of D-501 and D-502 under scheme B in comparison with [10].

Results	Pilot plant data[10]	Simulation results	Error (%)
D-501			
Distillate temperature (°C)	75	75.4	0.53
Distillate mass flow (g/h)	498	498	0.00
Product mass flow (g/h)	61	61	0.00
CH_3OH feed temperature (°C)	61	61	0.00
CH_3OH feed mass flow rate (g/h)	532	532.4	0.08
Water content in product (ppm)	60	24	60.00
CH_3OH in product (wt.%)	70	70	0.00
$NaOCH_3$ in product (wt.%)	30	30	0.00
D-502			
Distillate mass flow (g/h)	478	478	0.00
Bottom mass flow (g/h)	20	20	0.00
Water content in distillate (ppm)	30	4.1	86.33
CH_3OH content in bottom (wt.%)	1	0.2	80.00

Table 5. Initial operating condition of feed and distillation column (D-502) of $NaOCH_3$ synthesis under scheme B.

Parameters	Values
Pressure of process (atm)	1
NaOH solution feed flow rate (kg/h)	999.5
NaOH solution feed temperature (°C)	75
CH_3OH make-up feed temperature (°C)	30
D-502	
theoretical stages	30
Condenser	Partial-vapor
Distillate to feed ratio	0.8471
Reflux ratio	0.6456
Feed stage location	20

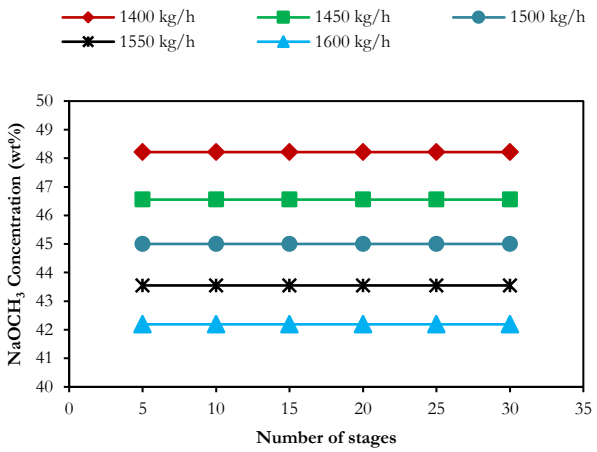

(a)

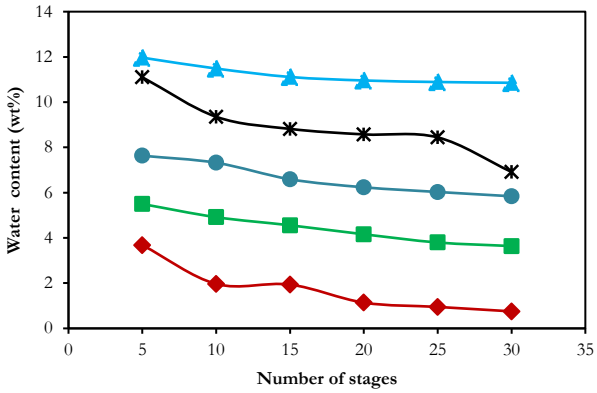

(b)

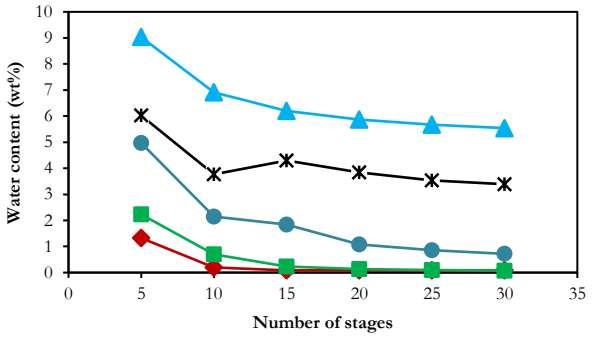

(c)

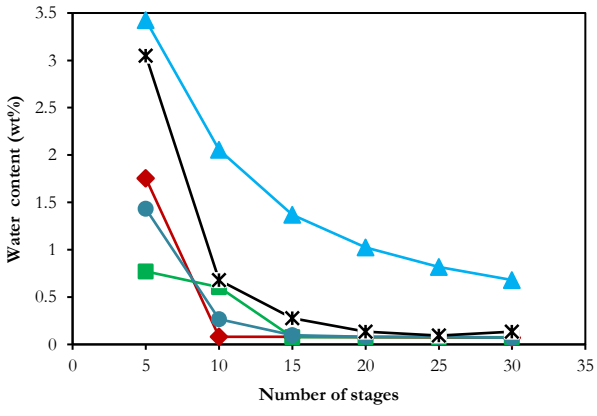

(d)

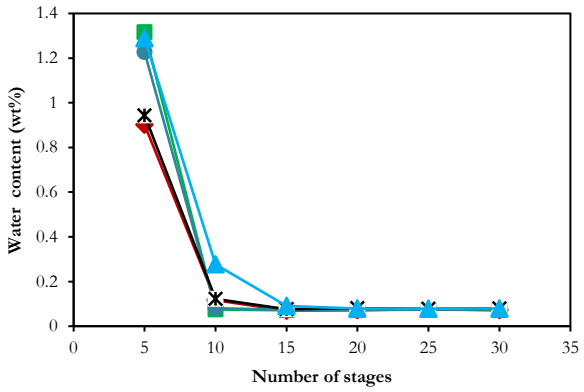

(e)

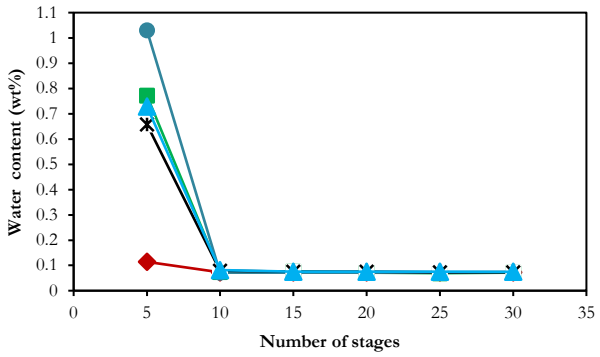

(f)

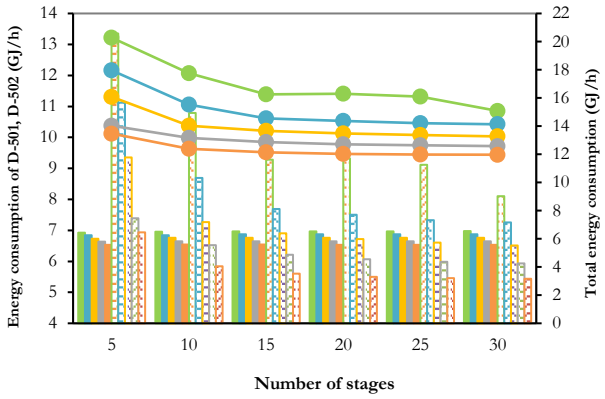

(a)

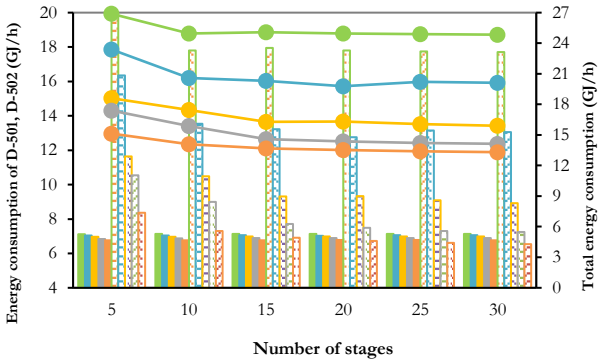

(b)

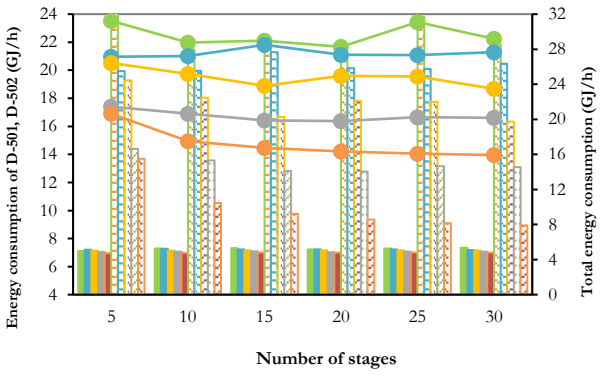

(c)

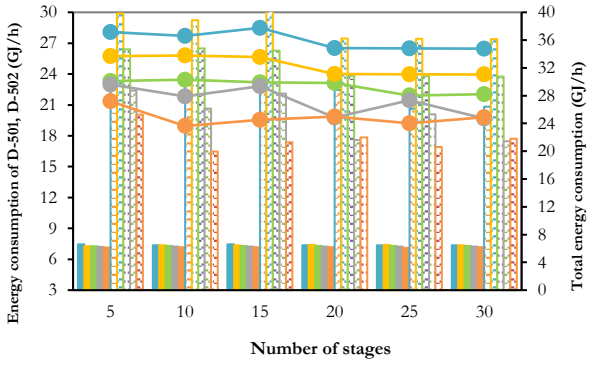

(d)

Fig. 5. The effect of number of stages and bottom flow rate (1400-1600 kg/h) of D-501 of scheme B on the concentration of: (a) $NaOCH_3$ (CH_3OH/NaOH ratio = 1.2 – 1.6), (b) water (CH_3OH/NaOH ratio = 1.2), (c) water (CH_3OH/NaOH ratio = 1.3), (d) water (CH_3OH/NaOH ratio = 1.4), (e) water (CH_3OH/NaOH ratio = 1.5), (f) water (CH_3OH/NaOH ratio = 1.6)).

Table 6. The optimal feed and product conditions of $NaOCH_3$ synthesis under scheme B.

Parameters	Values
NaOH solution feed flow rate (kg/h)	999.5
CH_3OH make-up feed rate (kg/h)	1,400
$NaOCH_3$ production (kg/h)	675 (43.55 wt.%)
D-501	
pressure (atm)	1
theoretical stages	25
Condenser	No condenser
Bottom rate (kg/h)	1,550
Feed stage location	1 (NaOH), 24 (CH_3OH)
Energy consumption (GJ/h)	35.13

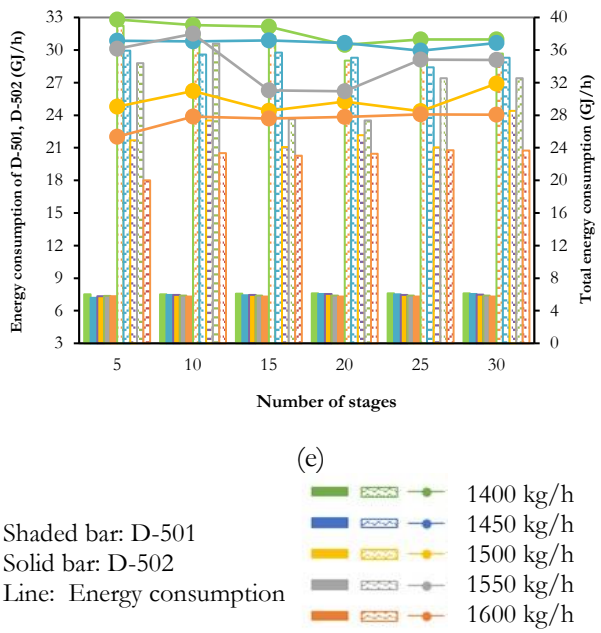

Fig. 6. The effect of number of stages (5-30) and bottom flow rate (1400-1600 kg/h) on the energy consumption of scheme B under CH_3OH/NaOH feed flow ratio of: (a) 1.2, (b) 1.3, (c) 1.4, (d) 1.5, (e) 1.6.

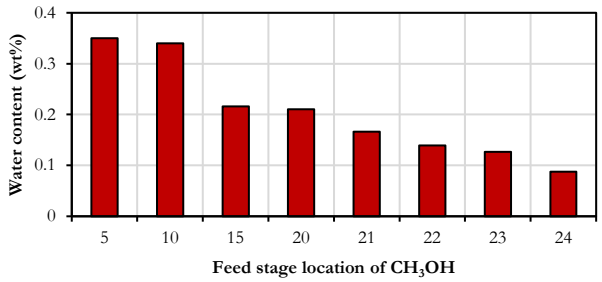

Fig. 7. The effect of CH_3OH feed stage location of D-501 of scheme B on water content, given CH_3OH/NaOH feed flow ratio of 1.4, bottom flow rate of 1,550 kg/h and the number of stage is 25.

3.3 Simulation Results under Scheme C

Figure 8 illustrates the schematic of $NaOCH_3$ synthesis under Scheme C, and Table 7 tabulates the initial operating conditions of feed and pervaporation membrane (PERVAP) of $NaOCH_3$ synthesis. The pervaporation membrane to separate CH_3OH from water was of A-type zeolite membrane due to high permeate flux, separation factor, and PSI [26].

Figure 9 illustrates the effect of number of stages (5-30) and bottom flow rate (1400-1600 kg/h) on $NaOCH_3$ concentration of D-501 under scheme C, given CH_3OH/NaOH feed flow ratios of 1.2, 1.3, 1.4, 1.5, and 1.6. The $NaOCH_3$ concentration was independent of the number of stages and CH_3OH/NaOH feed flow ratio. Meanwhile, the $NaOCH_3$ concentration was inversely correlated with the bottom flow rate. To maintain $NaOCH_3$ in liquid phase, the maximum concentration of $NaOCH_3$ was 45 wt%. In Fig. 9, the $NaOCH_3$ concentrations exceeded the 45 wt% maximum threshold under the bottom flow rates of 1400 and 1450 kg/h. The $NaOCH_3$ concentrations were below the maximum threshold for the bottom flow rates of 1500, 1550, and 1600 kg/h.

Figures 10 (a)-(b) depict the effect of number of stages (5-30) and bottom flow rate (1400-1600 kg/h) of D-501 under scheme C on the water content and energy consumption, given CH_3OH/NaOH feed flow ratio of 1.2. Given 0.01 wt% water content and maximum 45 wt% $NaOCH_3$, the CH_3OH/NaOH feed flow ratio of 1.2 was non-ideal.

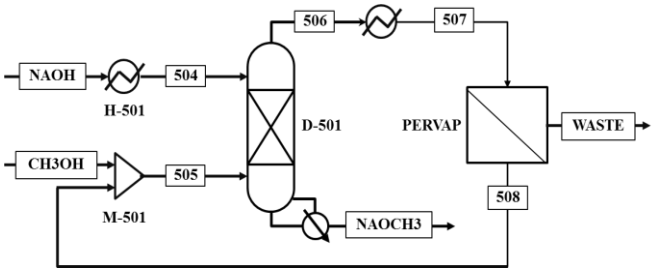

Fig. 8. The schematic of $NaOCH_3$ synthesis under scheme C.

Table 7 Initial operating conditions of feed and pervaporation membrane (PERVAP) of $NaOCH_3$ synthesis under scheme C.

Parameters	Values
Pressure (atm)	1
NaOH solution feed flow rate (kg/h)	999.5
NaOH solution feed temperature (˚C)	75
CH_3OH make-up feed temperature (˚C)	30
Type of membrane	A-type zeolite
Membrane area (m^2)	3.76
Temperature of pervaporation (˚C)	65

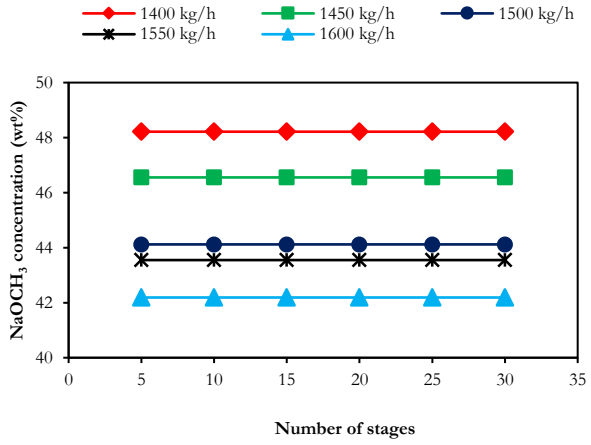

Fig. 9. The effect of number of stages (5-30) and bottom flow rate (1400-1600 kg/h) on $NaOCH_3$ concentration of D-501 under scheme C, given CH_3OH/NaOH feed flow ratios of 1.2, 1.3, 1.4, 1.5, and 1.6.

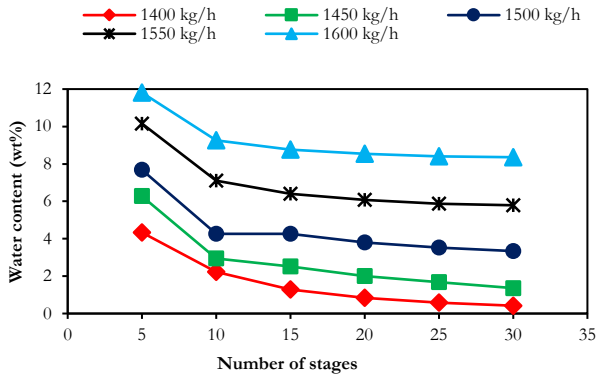

(a)

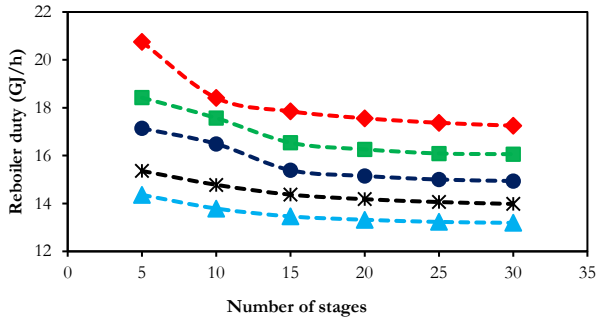

(b)

Fig. 10. The effect of number of stages (5-30) and bottom flow rate (1400-1600 kg/h) of D-501 under scheme C given CH_3OH/NaOH feed flow ratio of 1.2: (a) water content, (b) energy consumption.

Figures 11 (a)-(b) show the effect of number of stages (5-30) and bottom flow rate (1400-1600 kg/h) of D-501 under scheme C on the water content and energy consumption, given CH_3OH/NaOH feed flow ratio of 1.3. Likewise, the CH_3OH/NaOH feed flow ratio of 1.3 was non-ideal, given 0.01 wt% water content and maximum 45 wt% $NaOCH_3$.

Figures 12, 13, and 14 show the effect of number of stages (5-30) and bottom flow rate (1400-1600 kg/h) of D-501 under scheme C on the water content and energy consumption, given the CH_3OH/NaOH feed flow ratios of 1.4, 1.5, and 1.6, respectively. Given 0.01 wt% water content and maximum 45 wt% NaOCH3, the lowest total energy consumption (34.25 GJ/h) of D-501 under scheme C was achieved under the CH_3OH/NaOH feed flow ratio of 1.4, the bottom rate of 1550 kg/h, and the number of stages of 25 (Fig. 12 (b)).

The initial condition of pervaporation of scheme C was based on [24], and the values were validated by ASPEN Plus and the percentage errors tabulated Table 8. The simulation results and the reference were in good agreement despite small discrepancies of 0.01 % and 0.27 % for the separation factor and PSI.

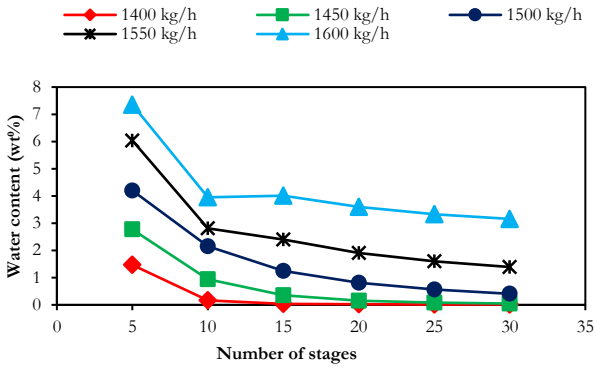

(a)

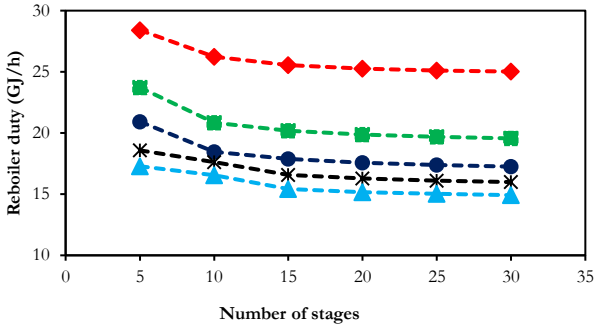

(b)

Fig. 11. The effect of number of stages (5-30) and bottom flow rate (1400-1600 kg/h) of D-501 under scheme C given CH_3OH/NaOH feed flow ratio of 1.3: (a) water content, (b) energy consumption.

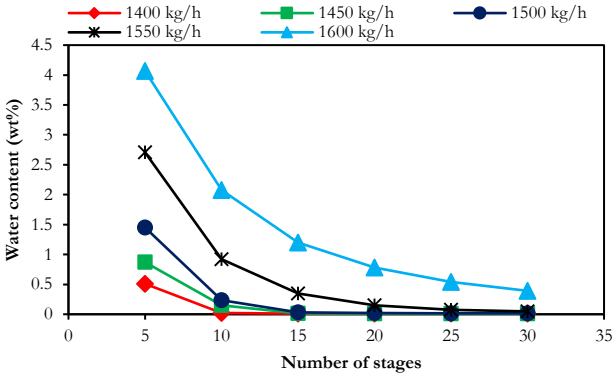

(a)

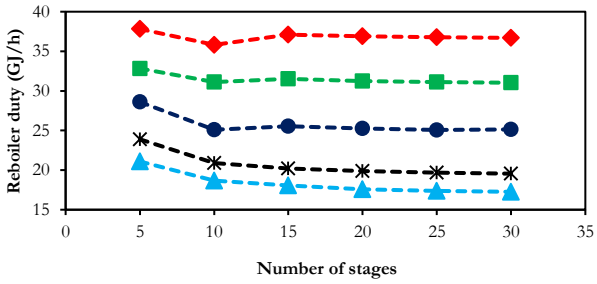

(b)

Fig. 12. The effect of number of stages (5-30) and bottom flow rate (1400-1600 kg/h) of D-501 under scheme C given CH_3OH/NaOH feed flow ratio of 1.4: (a) water content, (b) energy consumption.

DOI:10.4186/ej.2020.24.6.63

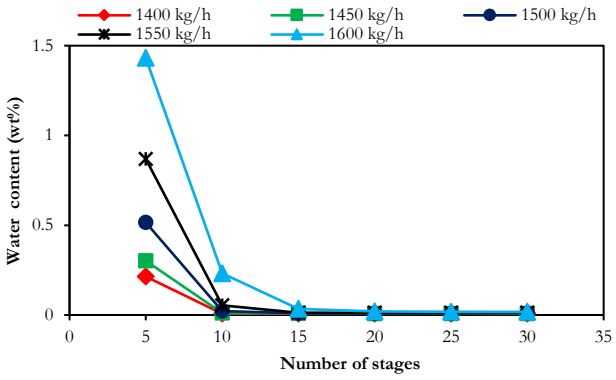

(a)

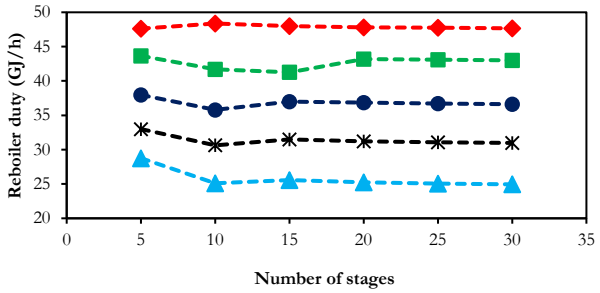

(b)

Fig. 13. The effect of number of stages (5-30) and bottom flow rate (1400-1600 kg/h) of D-501 under scheme C given CH_3OH/NaOH feed flow ratio of 1.5: (a) water content, (b) energy consumption.

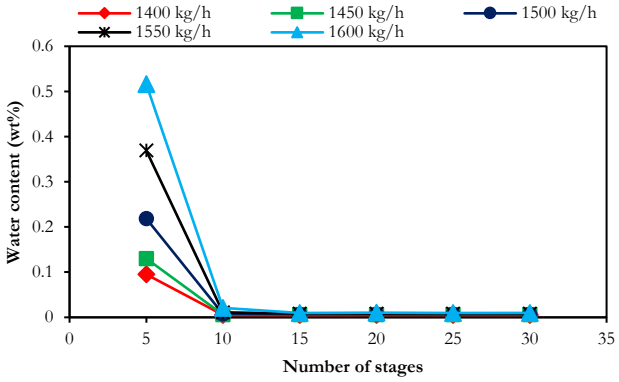

(a)

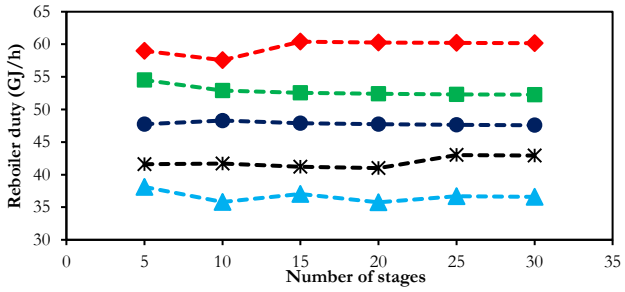

(b)

Fig. 14. The effect of number of stages (5-30) and bottom flow rate (1400-1600 kg/h) of D-501 under scheme C given CH_3OH/NaOH feed flow ratio of 1.6: (a) water content, (b) energy consumption.

Table 8. Comparison between the reference [24] and validation results on the pervaporation membrane.

	Reference data [24]	Validation results	Error (%)
Type of membrane	A-type zeolite	A-type zeolite	-
Temperature of feed (°C)	60	60	0
Permeate pressure (mbar)	7	7	0
Membrane area (cm^2)	60	60	0
Water feed (wt%)	10.1	10	0.99
Water permeate (wt%)	99.91	99.91	0
Permeate flux (kg/m^2h)	0.46	0.46	0
Separation factor	10000	9998.78	0.01
PSI (kg/m^2h)	4599.54	4611.81	0.27

Under scheme C, given the CH_3OH/NaOH feed flow ratio of 1.4, the bottom rate of 1550 kg/h, and the number of stages of 25 of D-501, the permeate flux was 2.68 x 10-3 kg/m2h, PSI was 26.75 kg/m2h, and the separation factor was 9991 (eq. (7)) since only one single pervaporation membrane was deployed in the scheme.

Figures 15 (a)-(e) illustrate the effect of number of stages (5-30) and bottom flow rate (1400-1600 kg/h) of D-501 of scheme C on the permeate flux of pervaporation membrane, given the CH_3OH/NaOH feed flow ratios of 1.2, 1.3, 1.4, 1.5, and 1.6. The number of stages and bottom flow rate were positively correlated with the permeate flux. The permeate flux decreased under the CH_3OH/NaOH feed flow ratios of 1.5 and 1.6. This could be attributed to lower water content as the CH_3OH/NaOH feed flow ratio increased.

Figures 16 (a)-(e) illustrate the effect of number of stages (5-30) and bottom flow rate (1400-1600 kg/h) of D-501 of scheme C on PSI of pervaporation membrane, given the CH_3OH/NaOH feed flow ratios of 1.2, 1.3, 1.4, 1.5, and 1.6. The PSI was positively related to the permeate flux. Table 9 tabulates the optimal feed, D-501, and pervaporation conditions of $NaOCH_3$ synthesis under scheme C.

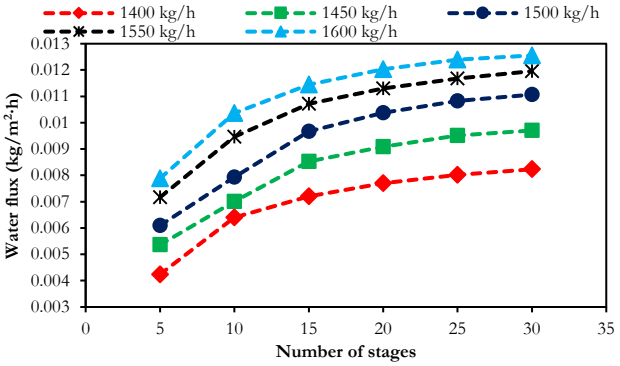

(a)

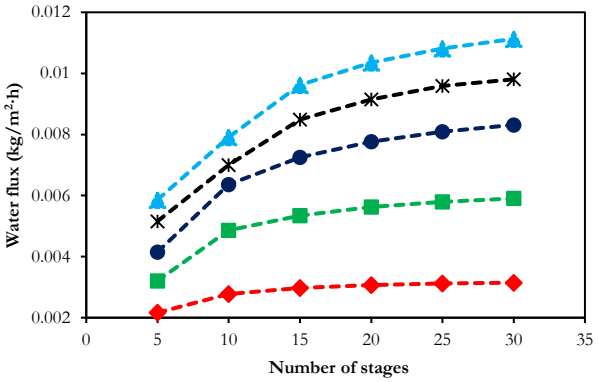

(b)

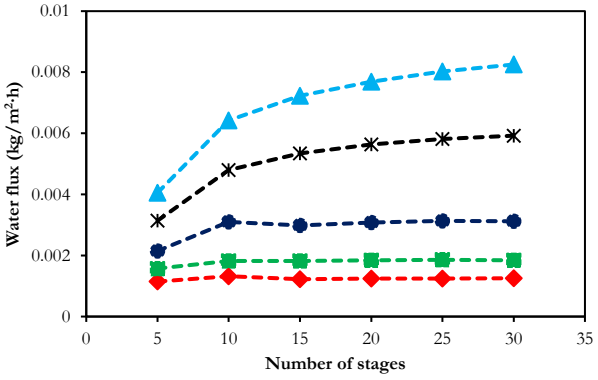

(c)

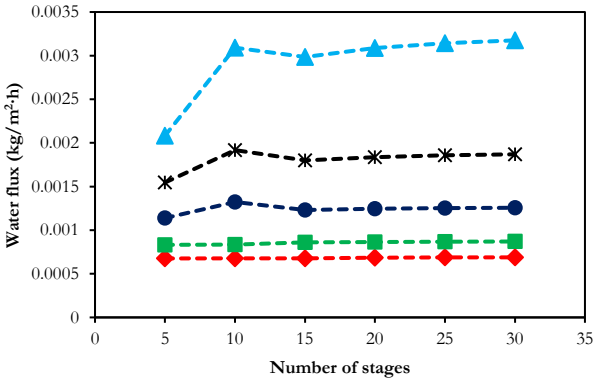

(d)

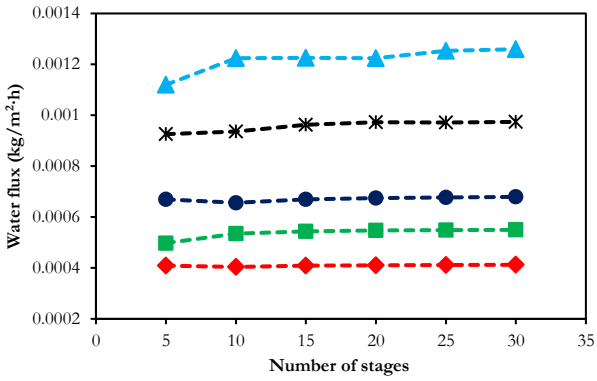

(e)

Fig. 15. Effect of number of stages (5-30) and bottom flow rate (1400-1600 kg/h) of D-501 of scheme C on the permeate flux of pervaporation membrane under CH_3OH/NaOH feed flow ratio of: a) 1.2, b) 1.3, c) 1.4, d) 1.5, e) 1.6.

3.4 Comparison between Synthetic Schemes

Under scheme A, the optimal $NaOCH_3$ synthetic condition (with 0.01 wt% water content, maximum 45 wt% $NaOCH_3$ and lowest energy consumption) was of CH_3OH/NaOH feed flow ratio of 4, the number of stages of 15, the bottom flow rate of 1550 kg/h, and the 14th feed stage location, with the $NaOCH_3$ flow rate of 675 kg/h. The total energy consumption under the optimal condition was 2229.37 GJ/h. The energy inefficiency was attributable to the reactor (Fig. 1).

The optimal $NaOCH_3$ synthesis condition under scheme B was of CH_3OH/NaOH feed flow ratio of 1.4, the number of stages of 25, the bottom flow rate of 1550 kg/h, and the 24th feed stage location, with the $NaOCH_3$ flow rate of 675 kg/h. The total energy consumption under the optimal condition was 35.13 GJ/h. The energy efficiency of scheme B was attributable to substituting the reactor with the reactive distillation column (D-501, Fig. 4).

Under scheme C, the optimal $NaOCH_3$ synthetic condition was of CH_3OH/NaOH feed flow ratio of 1.4, the number of stages of 25, the bottom flow rate of 1550 kg/h, and the 24th feed stage location, with the $NaOCH_3$ flow rate of 675 kg/h. The total energy consumption under scheme C was 34.25 GJ/h. The energy consumption of scheme C was slightly lower than under scheme B as a result of switching from the distillation column (D-502) to the pervaporation membrane. Nonetheless, the implementation of the pervaporation membrane in place of the distillation column to separate CH_3OH from water substantially lowered the capital cost of scheme C [30, 31], vis-à-vis scheme B. In essence, scheme C holds promising potential as an alternative for energy-efficient production of $NaOCH_3$.

DOI:10.4186/ej.2020.24.6.63

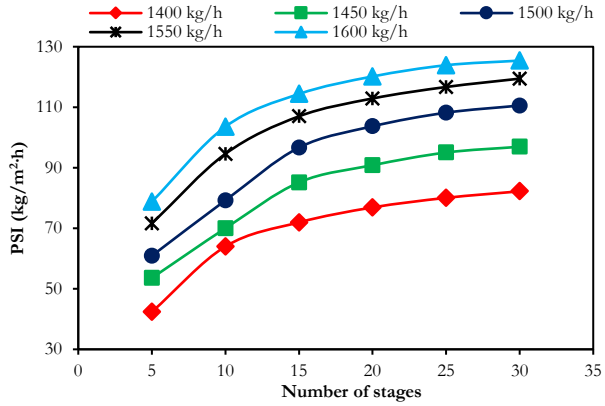

(a)

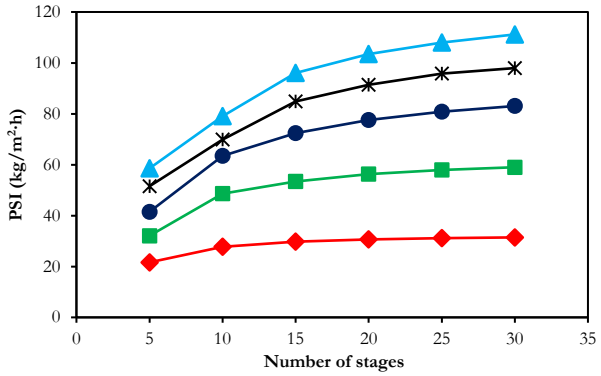

(b)

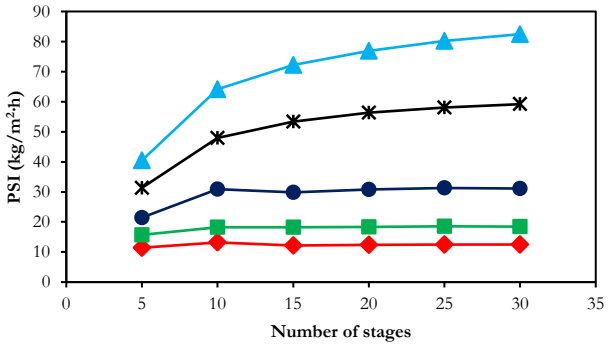

(c)

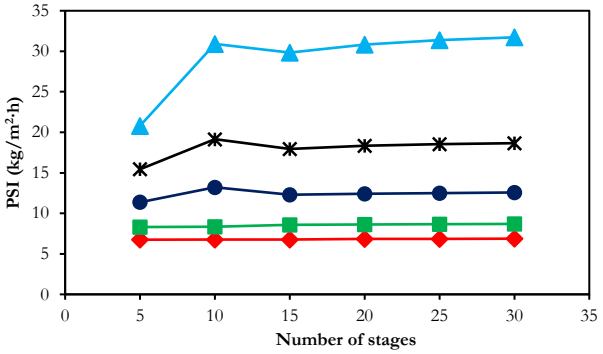

(d)

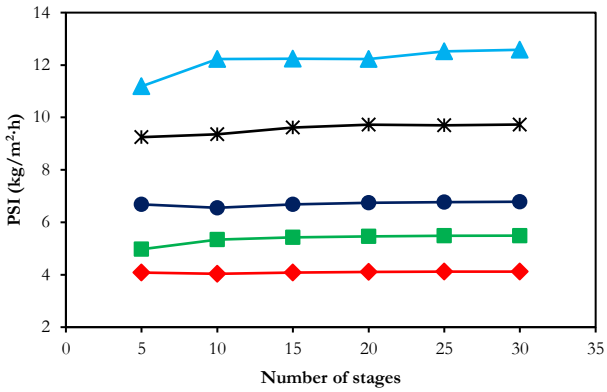

(e)

Fig. 16. Effect of number of stages (5-30) and bottom flow rate (1400-1600 kg/h) of D-501 of scheme C on PSI of pervaporation membrane under CH_3OH/NaOH feed flow ratio of: a) 1.2, b) 1.3, c) 1.4, d) 1.5, e) 1.6.

Table 9. The optimal feed, D-501, and pervaporation conditions of $NaOCH_3$ synthesis under scheme C.

Parameters	Values
NaOH solution feed rate (kg/h)	999.5
CH_3OH make-up feed rate (kg/h)	1,400
$NaOCH_3$ production (kg/h)	675 (43.55 wt.%)
D-501	
pressure (atm)	1
theoretical stages	25
Condenser	None condenser
Bottom rate (kg/h)	1,550
Feed stage location	24
Pervaporation	
Type of membrane	A-type zeolite
Pressure (atm)	1
Temperature of feed (T_F, °C)	65
Membrane area (m^2)	3.76
Water permeate (wt.%)	99.8
Water flux (kg/m^2h)	2.68×10^{-3}
Separation factor	9,991
PSI (kg/m^2h)	26.75

4. Conclusion

This research comparatively investigated the process simulation of $NaOCH_3$ synthesis from CH_3OH and NaOH under three synthetic schemes: schemes A, B, and C. Scheme A consisted of one equilibrium reactor and two distillation columns, scheme B one reactive distillation column and one distillation column, and scheme C one reactive distillation column and pervaporation membrane. Simulations were carried out by using ASPEN Plus. The simulation parameters

included CH_3OH/NaOH feed flow ratio (1.2-1.6), number of stages (5-30), bottom flow rate (1400-1600 kg/h), and feed stage location (5, 10, 15, 20, 21, 22, 23, and 24). The simulation parameters were varied to determine the optimal $NaOCH_3$ synthetic condition with 0.01 wt% water content, maximum 45 wt% $NaOCH_3$, and lowest total energy consumption. The results revealed that the optimal $NaOCH_3$ synthetic condition under scheme A was CH_3OH/NaOH feed flow ratio of 4, number of stages of 15, bottom flow rate of 1550 kg/h, and feed stage location of 14, with the total energy consumption of 2229.37 GJ/h. Under scheme B, the corresponding values were 1.4, 25, 1550 kg/h, and 24, with the total energy consumption of 35.13 GJ/h. Under scheme C, the optimal $NaOCH_3$ synthetic condition was CH_3OH/NaOH feed flow ratio of 1.4, number of stages of 25, bottom flow rate of 1550 kg/h, and feed stage location of 24, with the total energy consumption under scheme C was 34.25 GJ/h. Scheme C holds great potential as an energy-efficient alternative for synthesis of $NaOCH_3$. In subsequent research, the scope would be extended to incorporate the economic aspect of techno-economic assessment, in addition to the process simulation.

Acknowledgments

The authors would like to extend sincere appreciation to the National Science and Technology Development Agency (NSTDA) for the financial sponsorship under the "Research Chair Grant".

References

[1] K. S. Chen, Y. C. Lin, K. H. Hsu, and H. K. Wang, "Improving biodiesel yields from waste cooking oil by using sodium methoxide and a microwave heating system," *Energy*, vol. 38, no. 1, pp. 151-156, Feb. 2012.

[2] W. Shi, J. Li, B. He, F. Yan, Z. Cui, K. Wu, L. Lin, X. Qian, and Y. Cheng, "Biodiesel production from waste chicken fat with low free fatty acids by an integrated catalytic process of composite membrane and sodium methoxide," *Bioresour. Technol.*, vol. 139, pp. 316-322, Jul. 2013.

[3] Y. C. Lin, K. H. Hsu, and J. F. Lin, "Rapid palm-biodiesel production assisted by a microwave system and sodium methoxide catalyst," *Fuel*, vol. 115, pp. 306-311, Jan. 2014.

[4] T. Kai, G. L. Mak, S. Wada, T. Nakazato, S. Takanashi, and Y. Uemura, "Production of biodiesel fuel from canola oil with dimethyl carbonate using an active sodium methoxide catalyst prepared by crystallization," *Bioresour. Technol.*, vol. 163, pp. 360-363, Apr. 2014.

[5] Q. Kwok, B. Acheson, R. Turcotte, A. Janes, and B. Marliar, "Fire and explosion hazards related to the industrial use of potassium and sodium methoxides," *J. Hazard.*, vol. 250-251, pp. 484-490, Apr. 2013.

[6] X. Lv, J. Lin, L. Luo, D. Zhang, S. Lei, W. Xiao, Y. Xu, Y. Gong, and Z. Liu, "Enhanced enzymatic saccharification of sugarcane bagasse pretreated by sodium methoxide with glycerol," *Bioresour. Technol.*, vol. 249, pp. 226-233, Feb. 2018.

[7] J. F. O. Granjo and N. M. C. Oliveira, "Process simulation and techno-economic analysis of the production of sodium methoxide," *Ind. Eng. Chem.*, vol. 55, no. 1, pp. 156-167, Jan. 2016.

[8] R. G. Adams, T. V. Bommaraju, and S. D. Fritts, "Method of denuding sodium mercury amalgam and producing sodium alcoholates," U.S. Patent 5,262,133, Nov. 16, 1993.

[9] S. W. Tse, "Continuous process for sodium methylate," U.S. Patent H001697, Nov. 4, 1997.

[10] J. Guth, H. Friedrich, H. J. Sterzel, G. Kaibel, K. Burkart, and E. Hoffmann, "Method for producing alkali methylates," U.S. Patent 6759560, Jul. 6, 2004.

[11] R. Taylor and R. Krishna, "Modelling reactive distillation," *Chem. Eng. Sci.*, vol. 55, pp. 5183-5229, Nov. 2000.

[12] S. Kai and K. Achim, *Reactive Distillation - Status and Future Directions Industrial Applications of Reactive Distillation*. Morlenbach, Germany: Wiley-VCH, 2002, pp. 308.

[13] S. J. Wang, C. C. Yu, and H. P. Huang, "Plant-wide design and control of DMC synthesis process via reactive distillation and thermally coupled extractive distillation," *Comput. Chem. Eng.*, vol. 34, no. 3, pp. 361-373, Mar. 2010.

[14] M. Zahrul, Rochmadi, Sutijan, and B. Arief Budiman, "Synthesis acetylation of glycerol using batch reactor and continuous reactive distillation column," *Eng. J.*, vol. 18, no. 2, pp. 29-39, Apr. 2014.

[15] E. S. Pérez-Cisneros, X. Mena-Espino, V. Rodriguez-Lopez, M. Sales-Cruz, T. Viveros-Garcia, and R. Lobo-Oehmichen, "An integrated reactive distillation process for biodiesel production," *Comput. Chem. Eng.*, vol. 91, pp. 233-246, Aug. 2016.

[16] S. J. Parulekar, "Analysis of pervaporation-aided esterification of organic acids," *Ind. Eng. Chem.*, vol. 46, pp. 8490-8504, Oct. 2007.

[17] B. L. Yang and S. Goto, "Pervaporation with reactive distillation for the production of ethyl tert-butyl ether," *Sep. Sci. Technol.*, vol. 32, no. 5, pp. 971-981, 1997.

[18] F. Aiouache and S. Goto, "Reactive distillation-pervaporation hybrid column for tert-amyl alcohol etherification with ethanol," *Chem. Eng. Sci.*, vol. 58, no. 12, pp. 2465-2477, Jun. 2003.

[19] V. Sukwattanajaroon, S. Charojrochkul, W. Kiatkittipong, A. Arpornwichanop, and S. Assabumrungrat, "Performance of membrane-assisted solid oxide fuel cell system fuelled by bioethanol," *Eng. J.*, vol. 15, no. 2, pp. 53-66, Apr. 2011.

[20] S. Theerawat, P. Panu, P. Kerdlarpphon1, N. Rungpeerapong, V. Burapatana, and M. Phisalaphong, "Bacterial cellulose-alginate membrane for dehydration of biodiesel-methanol mixtures," *Eng. J.*, vol. 20, no. 5, pp. 145-153, Nov. 2016.

[21] M. Juhani, *Hydroxide−Alkoxide Ion Equilibria and Their Influence on Chemical Reactions. Chemistry of Functional Groups*. 1971. Available: http://onlinelibrary.wiley.com [Accessed: 22 June 2019]

[22] B. H. Li, N. Zhang, and R. Smith, "Simulation and analysis of CO_2 capture process with aqueous monoethanolamine solution," *Appl. Energy*, vol. 161, pp. 707-717, Jul. 2016.

[23] D. Bacovsky, W. Korbitz, M. Mittelbach, and M. Worgetter, "Biodiesel production: Technologies and European providers," IEA Task 39, Rep. T39-B6, 2007.

[24] S. Sommer, and T. Melin, "Performance evaluation of microporous inorganic membranes in the dehydration of industrial solvents," *Chem. Eng. Process.*, vol. 44, pp. 1138-1156, Oct. 2005.

[25] M. Yoshikawa, K. Masaki, and M. Ishikawa, "Pervaporation separation of aqueous organic mixtures through agarose membranes," *J. Membr. Sci.*, vol. 205, no. 1-2, pp. 293-300, Aug. 2002.

[26] X. Liu, Y. Sun, and X. Deng, "Studies on the pervaporation membrane of permeation water from methanol/water mixture," *J. Membr. Sci.*, vol. 325, no. 1, pp. 192-198, Nov. 2008.

[27] S. Bano, A. Mahmood, and K. H. Lee, "Vapor permeation separation of methanol–water mixtures: Effect of experimental conditions," *Ind. Eng. Chem.*, vol. 52, no. 31, pp. 10450-10459, Feb. 2013.

[28] P. Aptel, N. Challard, J. Cuny, and J. Neel, "Application of the pervaporation process to separate azeotropic mixtures," *J. Membr. Sci.*, vol. 1, pp. 271-287, Feb. 1976.

[29] S. Sommer and T. Melin, "Influence of operation parameters on the separation of mixtures by pervaporation and vapor permeation with inorganic membranes. Part 1: Dehydration of solvents," *Chem. Eng. Sci.*, vol. 60, no. 16, pp. 4509-4523, Aug. 2005.

[30] D. Kunnakorn, T. Rirksomboon, K. Siemanond, P. Aungkavattana, N. Kuanchertchooc, P. Chuntanalerg, K. Hemra, S. Kulprathipanja, R. B. James, and S. Wongkasemjita, "Techno-economic comparison of energy usage between azeotropic distillation and hybrid system for water ethanol separation," *Renew. Energy*, vol. 51, pp. 310-316, Mar, 2013.

[31] M. C. Daviou, P. M. Hoch, and A. M. Eliceche, "Design of membrane modules used in hybrid distillation/pervaporation systems," *Ind. Eng. Chem. Res.*, vol. 43, no.13, pp. 3403-3412, May 2004.

Natthiyar Aeamsuksai, photograph and biography not available at the time of publication.

Thirawat Mueansichai, photograph and biography not available at the time of publication.

Pongtorn Charoensuppanimit, photograph and biography not available at the time of publication.

Pattaraporn Kim-Lohsoontorn, photograph and biography not available at the time of publication.

Farid Aiouache, photograph and biography not available at the time of publication.

Suttichai Assabumrungrat, photograph and biography not available at the time of publication.